Granular Matter (2017) 19:21
DOI 10.1007/s10035-017-0703-z

ORIGINAL PAPER

Manifestation of particle morphology on the mechanical behaviour of granular ensembles

Ramesh K. Kandasami[1] · **Tejas G. Murthy**[1]

Received: 10 September 2015 / Published online: 23 February 2017

Abstract This paper presents the effect of particle morphology (grain shape) on the mechanical response of granular materials. Two model systems with extreme differences in morphology were selected (spherical glass ballotini and angular sand) for this experimental programme. A series of hollow cylinder torsion tests were conducted in this programme under monotonic drained conditions on specimens reconstituted to the same relative density. Tests were conducted under different intermediate principal stress ratio (b) on both the model materials. The glass ballotini shows increased dilation at the outset of the test, however, at large strains, the particle rearrangement in the sand and the increased interlocking leads to higher strength at the critical state. The effect of individual particle morphology is manifested in both the increased friction angle and a larger sized failure locus in stress space with increase in angularity. The stresses developed in these two model materials are also accompanied by intriguing volume change behaviour. The glass ballotini despite a lower strength presents a predominantly dilative response immaterial of the 'b' value, while the angular sand shows increased strength at large strains, while showing a contractive response. These results allow incorporation of particle morphology effects at the ensemble level in plasticity based constitutive models.

✉ Tejas G. Murthy
tejas@civil.iisc.ernet.in; tejasgm@gmail.com

Ramesh K. Kandasami
rameshkk@civil.iisc.ernet.in; ramesh.k.kannan@gmail.com

[1] Department of Civil Engineering, Indian Institute of Science, CV Raman Avenue, Bangalore 560012, India

Keywords Particle shape · Dilatancy · Intermediate principal stress · Failure locus

1 Introduction

Granular materials (eg. soils, powders) are a collection of solid particles, in which most of them are in contact with at least few of its neighboring particles [1]. At an ensemble level, the mechanical behaviour is a cumulative response of individual inter-grain interactions. It has been long recognized [2] that the physical properties of an individual particle such as shape or morphology has an influence on the overall ensemble mechanical response such as the internal friction, permeability, compressibility, shear strength etc. The morphological characteristics of individual particulates are described through three independent geometric or shape descriptors [3] such as form or sphericity, roundness, surface texture or roughness. Even though there are several derivatives of these independent shape descriptors such as non-convexity, inverse aspect ratio etc. [4], the three independent shape descriptors form the basis of any morphological characterization. Cavaretta [5] provides a very detailed account of the techniques used for estimating the various morphological parameters for individual particles. Techniques using optical imaging, electron microscopy and subsequent Fourier analysis or fractal analysis of these images have broadened the suite of methods available for comprehensive morphological characterization of the individual particulates.

Almost all the features of mechanical response of a granular ensemble are affected by the individual particle morphology as observed through extensive experiments. The maximum and minimum packing fractions (density or void ratio—detailed in "Appendix") change significantly with par-

ticle shape; angular particles show a large difference between the maximum and minimum densities, while spherical particles show very less difference [6–8]. Santamarina and Cho [9] while characterizing particle morphology have also enumerated inter-grain interactions such as sliding, rolling, interlocking etc. that reflects in the ensemble mechanical behavior in all strain regimes. In the small strain regime, the stiffness and shear wave velocity increases with increase in angularity [10]. At a given relative density, angular particles show increased strength (and mobilized friction angle) than rounded particles as observed in conventional laboratory tests (such as triaxial compression tests, direct shear tests etc.) [4,11]. Tests performed under constant volume conditions showed that the rounded sands were more unstable and had lower strength than the angular sands [12]. Under large deformations, friction angle at the critical state (CS), critical state intercept (e vs. log p′), peak friction angle, and friction angle mobilized at the onset of dilation all of them increase with increase in angularity [11,13].

Advances in the understanding of granular material behaviour through specialized laboratory testing (such as true triaxial and hollow cylinder torsion—HCT) have underscored the importance of "fabric". Fabric at a continuum scale is described as the particle arrangement (bedding plane of deposition) vis-à-vis the inclination of principal stresses which results in an anisotropic behavior of a granular ensemble. This anisotropy is due to the dual effects of particle arrangement (called inherent anisotropy) and loading direction with respect to the deposition plane (called induced anisotropy) [14–17]. A dimensionless parameter '*b*', (which can also be associated with the Lode angle—[18–20]), is often used to depict the effect of intermediate principal stress and map the failure locus on the octahedral plane. The equation, which defines the parameter '*b*' also called intermediate principal stress ratio, is given below.

$$b = \frac{\sigma'_2 - \sigma'_3}{\sigma'_1 - \sigma'_3} \tag{1}$$

where σ'_1, σ'_2 and σ'_3 are major, intermediate and minor effective principal stresses.

Exploring the effect of this '*b*' through elemental tests (such as HCT tests and true triaxial tests) has been used to experimentally arrive at the shape of a yield surface [21,22]. Yield/Failure, which are mapped on to the octahedral or deviatoric (plane perpendicular to the hydrostatic axis), have been used in designing constitutive models of various levels of complexity (for example, bounding surface models, critical state models etc.). More recently, the effect of fabric has also been included through an evolving anisotropic fabric tensor [23,24]. Even though it is reasonably intuitive that the fabric in granular materials would depend on the individual particle morphology, experimental investigations on the effect particle morphology and its correspondence to the fabric of the particulate ensemble have been very few. To this end, recently, Yang [25] and Yang et al. [26] used a HCT testing apparatus to investigate the effect of particle morphology with varying principal stress inclination (α—defined in Eq. 5). Their results have shown that the anisotropy and non-coaxiality of granular solids is strongly affected by the individual particle morphology.

On the other hand discrete element method (DEM) has emerged as an invaluable tool for understanding the manifestations of individual particle morphology and the up-scaling (or coarse graining) to an ensemble level [27]. Strategies to create particles of various morphologies in DEM simulations have been extensively reported. Assemblages of particulates of various shapes have been simulated to understand the effect of these micro-level features on the macro (continuum) response of the ensemble [28,29]. Simulations in 2D packings of disks and elongated particles have revealed some very interesting force chain network signatures, while also indicating that elongated particles show increased shear strength and anisotropy [29–33]. Further, simulations in 3D packings have revealed that critical state strength, critical angle of internal friction of these ensembles increase as the particles become more angular (non-convex) [34–36]. This increased strength of angular particle assemblages compared to that of the spherical particles is a result of the rotational frustration [30] and increase in the coordination number [28,36]. These DEM simulations have also provided unparalleled insights into anisotropy of granular materials. With increase in angularity of the particles, the combined effect of fabric and force anisotropy contributes to greater strength of the assemblages [34–36]. DEM simulations investigating the effect of intermediate principal stresses on peak strength has been reported for particulate systems with different inter particle friction values. The particles with increased friction values showed an increase in peak strength at different '*b*' [37].

We present an experimental study to understand how variation in particle morphology manifests itself at a continuum or ensemble scale in granular material response. In order to understand this continuum response, we carried out a series of hollow cylinder torsion tests on two model particulate systems with very different particle morphology, spherical glass ballotini and very angular silica sand. These two model systems occupy two extreme corners of the Krumbien scale. The model granular ensembles were reconstituted to the same relative density (generally used as a descriptor of the state or packing of an ensemble—[38]) and consolidated to the same effective stress. We map the failure locus (or the critical state locus) of the two model systems through HCT tests conducted at various '*b*' values. These experiments allowed an exploration of the failure (yield) surface of the ensemble, in effect providing a continuum manifestation of the particle morphology. Ancillary inferences on the effect of individual

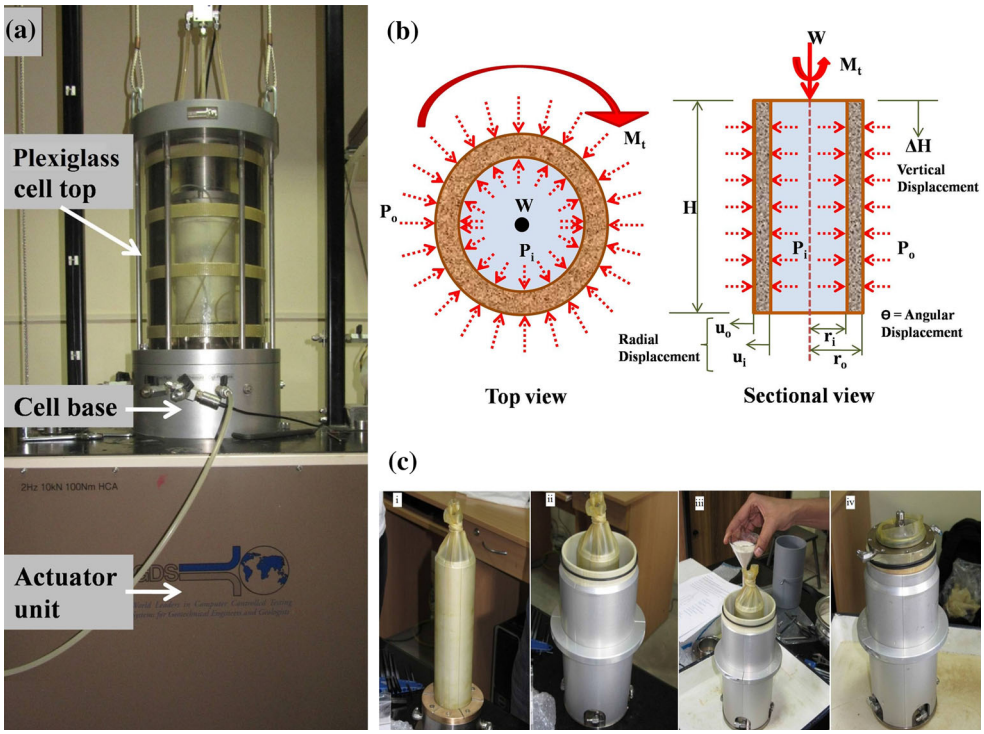

Fig. 1 **a** The hollow cylinder torsion testing apparatus with the actuator unit and the cell base used in this testing programme. **b** Schematic of the sectional view of the hollow cylindrical specimen subjected to load (W), torque (M_T), internal (P_i) and external (P_o) pressures. **c** Specimen reconstitution stages using water pluviation method

particle morphology on the internal friction angle, stress–dilatancy, non-coaxiality, and anisotropy are explored in this paper. This data set provides the experimental foundation for designing and benchmarking of continuum constitutive models that are necessary for solving engineering boundary value problems. Additionally, it also provides an extensive data set which will be useful in understanding and benchmarking DEM simulations that are traditionally performed on spherical particles and means for extending to other particle morphologies.

2 Experimental

A HCT testing system with fully automated controls (GDS Instruments Co., UK) was used in this study. We conducted a series of monotonic static drained tests to investigate the effect of intermediate principal stress ratio (b) and principal stress inclination (α). This HCT apparatus (shown in Fig. 1a) provided an independent control of the axial load (W), torque (M_T), internal (P_i) and external (P_o) pressures. The load cell, torqueducer and digital pressure volume controllers had a maximum capacity of 10 kN, 100 Nm and 2 MPa; the resolution of these sensors were 1 N, 0.008 Nm and 1 kPa respectively. The load, displacements and pressures were recorded at a rate of 0.1 Hz. Further details of the apparatus, instrumentation, actuation and measurement can be found elsewhere [22,39]. Figure 1b shows the section of the hollow cylinder specimen when subjected to boundary load, torque, P_i and P_o. Varying the load, torque and pressures, the four stress components (axial stress—σ_z, radial stress—σ_r, tangential stress—σ_θ and shear stress $\tau_{\theta z}$) are controlled independently. The ability to control these four stress components independently in turn allows control of the direction and magnitude of the principal stresses. The average stress components and the strain components acting on a continuum element are obtained by solving the balance equations [40]. The equations of these stress and strain components are given in the "Appendix".

3 Material characterization

Two model materials with significantly different particle morphologies were chosen for the study without fines or silt sized particles i.e. spherical glass ballotini and very angular quartzitic sand. The physical properties of the model materials are presented in Table 1. These model materials lie on the two extremes of the spectrum of particle morphologies [41–43]. The form/sphericity (S) of these two material systems was obtained by imaging about 20 particles using a scanning

Table 1 Physical properties of the model materials used

	Glass ballotini	Angular sand
Max. void ratio	0.73	0.97
Min. void ratio	0.60	0.53
Max. porosity	42.0%	49.0%
Min. porosity	37.5%	35.0%
Roudness (R)	0.97	0.17
Sphericity (S)	0.96	0.42
Roughness (R_a)	0.03	0.036
Specific gravity	2.50	2.65
Mean grain size (D_{50})	0.45 mm	0.45 mm
Uniformity coefficient (C_u)	2.80	3.20
Coefficient of curvature (C_c)	0.90	0.80

electron microscope and calculating the ratio of the radius of largest inscribed circle to the radius of smallest circumscribed circle for each particle thereby calculating an average value of S. Similarly the roundness (R) was also quantified from the average radius of curvature obtained from the surface irregularities to the radius of the maximum circle that can be inscribed in the particle/grain [8]. Figure 2a, b presents the scanning electron micrographs of the model materials used in this study. The particle roughness was characterized using a surface profilometer [44]. It was observed that the roughness values of two material systems were found to be 0.03 and 0.036 for glass ballotini and sand respectively. The effect of surface roughness on the overall mechanical response of these two model granular materials was negligible while sphericity and roundness forms a dominant factor. The mean grain size (D_{50}) of the two material systems was 0.45 mm while the coefficient of uniformity (C_u) and the coefficient of curvature (C_c) (equations given in the "Appendix") for both the material systems is provided in the Table 1. It should be noted here that when the uniformity coefficient is less than 4 the ensemble is said to have uniform or similarly sized particles. The differences in the mechanical response of these two model systems can be attributed to variations in particle morphology and not due to the gradation because the D_{50}, Cu and Cc are almost equal. The other physical characteristics such as specific gravity [45], maximum and minimum porosity, void ratio (definitions given in the "Appendix") [46,47] are also measured for the two material systems and shown in Table 1. The chemical characterization of these two materials, investigated using X-ray diffraction revealed that these materials were predominantly made of silica.

4 Specimen reconstitution

The HCT test specimens were reconstituted such that the relative densities (at the end of isotropic consolidation, i.e. prior to the shearing stage) are equal. Figure 1c shows the stages of artificial reconstitution of granular hollow cylinder specimens using water pluviation technique. This pluviation technique was used [48,49] to target a particular packing/density. Further details of the specimen reconstitution technique are provided in [39]. The dimensions of the specimen used in this study were 200 mm height, external diameter of 100 mm and internal diameter of 60 mm. These dimensions were fixed based on the criteria (given in the "Appendix") put forth by Sayao and Vaid [50] after extensive numerical simulations performed on a thick cylinder with different boundary conditions using both elastic and plastic formulations. The specimen geometry is fixed such that the stress distribution across the annulus is kept as uniform as possible.

The specimens were saturated with a backpressure of 300 kPa at an effective stress of 100 kPa until the Skempton B parameter [51] reached a value of 0.96 or more. All the specimens were isotropically consolidated to an effective stress of about 300 kPa in several stages, to achieve a target relative density of about 34% before shearing the specimen. Stress controlled monotonic drained tests (sheared at a rate of 1.5 kPa/min) were conducted at different values of intermediate principal stress ratio (b) keeping the major principal stress

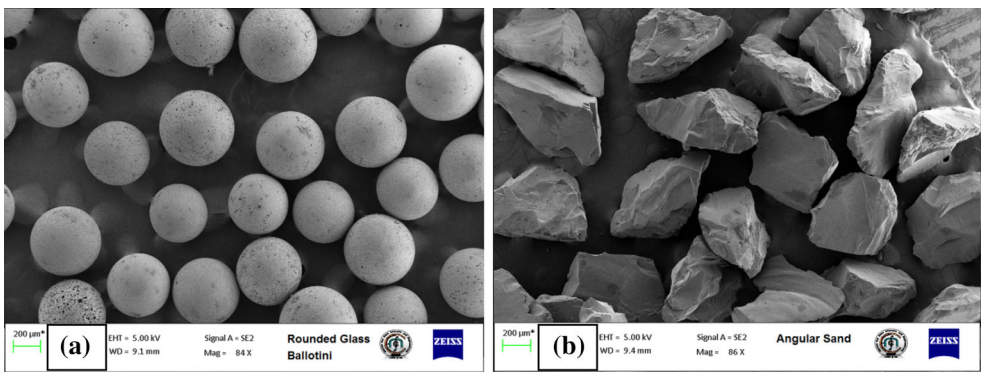

Fig. 2 Scanning electron micrographs of the two model materials used in this study. **a** Glass ballotini. **b** Sand

inclination (α) to be vertical. Two tests were also performed keeping $b = 0$ and $\alpha = 0° \,\&\, 90°$ for each model material system. Tests performed at different 'b' values other than $b = 0$ require varying the external and internal pressures of a hollow cylinder. Ratio of internal pressure (P_i) to external pressure (P_o) was maintained between 0.75 to 1.30 so that the stress non-uniformities developed during testing were minimal and acceptable [40,52,53]. This ratio of internal pressure (P_i) to external pressure (P_o) at the end of each test is given in the "Appendix" for the tests performed on both sand and glass ballotini. Errors due to membrane penetration were also calculated and observed to be negligible. A series of three tests were performed under the same stress conditions and fabric to check for repeatability. It was observed that the tests were highly repeatable.

5 Results

A series of 14 HCT tests (seven each on glass ballotini and sand were performed) results are analysed in the critical state soil mechanics framework (The CSSM is a conceptual framework built on the fundamentals of the mathematical theory of continuum plasticity, which elegantly combines the effect of density, mean effective stress, and shear stress on the plastic flow of a granular material [18,54]). In order to isolate the effect of particle morphology, two model systems were chosen which had identical particle size distribution and surface roughness. The specimens were then reconstituted to the same relative density, and consolidated to the same mean effective stress. A typical stress strain curve obtained for a test with $b = 0$ and $\alpha = 0°$, for glass ballotini and sand is presented in Fig. 3a, b, octahedral shear stress (scalar representation of the three dimensional stress given in the Eq. 23 of "Appendix") versus octahedral shear strain (Eq. 27 of "Appendix") between the two systems shows striking similarity i.e. the nonlinear increase in stress with strain and reaches a constant value at larger strains. However stresses reached at critical state of these two model systems is different. Sand exhibited a greater critical state stress of 206 kPa compared to that of glass ballotini (160 kPa). The volume change responses measured in the two systems show a significant difference, with the sand showing a predominantly contractive response while the glass ballotini showing a predominantly dilative response. The octahedral shear strain required to reach a critical state was larger for angular sands when compared to that of the rounded glass ballotini. All specimens had low packing fractions, which prevented severe localization, and allowed shearing to large strains. The specimen was deemed to have reached a 'critical state' when the octahedral shear stress and the volumetric strain reached a constant value under large deformation.

Some specimens continue to contract or dilate with continued shearing, and may sometimes show increased propensity for localization (or shear banding) without reaching a critical state. In such cases, we use the stress–dilatancy relation provided by Been and Jefferies [55] to identify the critical state, i.e., when the dilatancy $D_p = 0$, the corresponding stress ratio was considered as the critical state. The stress ratio (η) and dilatancy (D_p) are given in the Eqs. 2 and 3 below.

$$\eta = \frac{q}{p'} \tag{2}$$

$$D_p = \frac{\left(\varepsilon_{v,j+1} - \varepsilon_{v,j-1}\right) - \left(p'_{j+1} - p'_{j-1}\right)/K}{\left(\varepsilon_{q,j+1} - \varepsilon_{q,j-1}\right) - \left(q_{j+1} - q_{j-1}\right)/3G} \tag{3}$$

where the evolving dilatancy is computed through a central-difference performed on q (deviatoric stress), p′ (mean effective stress), ε_v (volumetric strain) and ε_q (deviatoric strain or shear strain) (equations of q, p′, ε_v, ε_q are provided in the appendix). K and G are bulk and shear modulus, which were obtained from experiments using resonant column apparatus for both the model materials reconstituted to the same relative density and confining pressure. The contri-

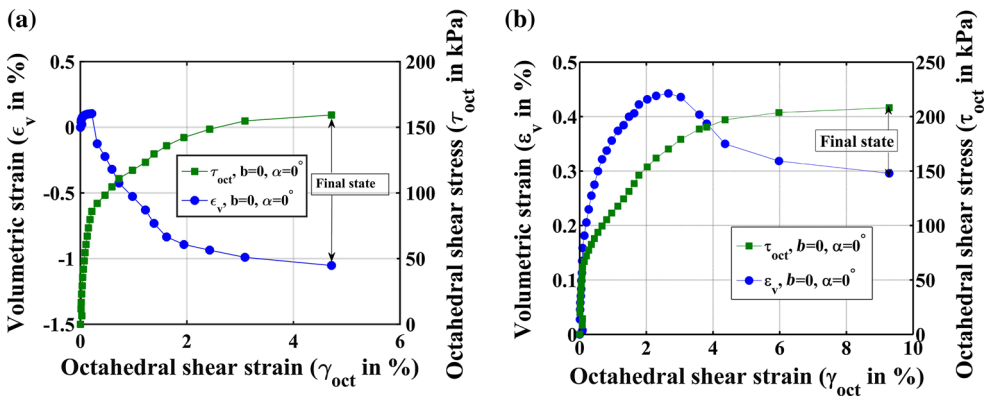

Fig. 3 Typical octahedral shear stress versus octahedral shear strain and volumetric strain plot for the two model materials. **a** Glass ballotini, where the volumetric strain is purely dilative. **b** Sand, where the volumetric strain is predominantly contractive

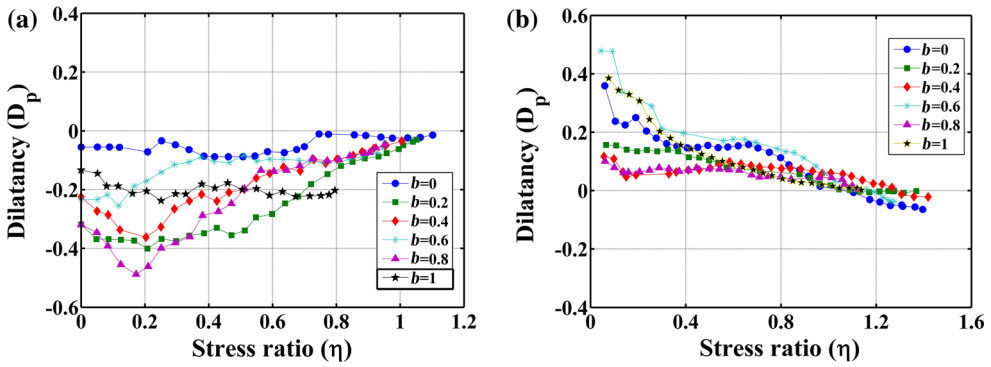

Fig. 4 Variation of dilatancy with increase in stress ratio for the two model material systems. **a** Glass ballotini—the behavior is predominantly dilative. The test at $b = 1$ did not reach a critical state. **b** Sand—the behavior is predominantly contractive

bution of the elastic strains is relatively small in calculating the plastic dilatancy, and hence a constant value of the elastic modulus was used.

Figure 4a, b shows the variation of dilatancy with stress ratio for 'b' values from 0 to 1 at 0.2 intervals for glass ballotini and sand respectively. As stated earlier, when the dilatancy values reaches almost 0, the specimens were considered to have reached a critical state (tests at $b = 1$ did not reach a clear critical state and the pressure ratio is very high). Even though some of the specimens did not reach the very large strains generally ascribed for a critical state, we conjecture that the stresses, friction angle measured in these tests, would not be significantly different and would not alter any conclusions if the specimens were to be sheared to very large strains. The dilatancy values are positive in case of sands due to its continued contractive response while the values are negative in case of dilative glass ballotini, also reported in the results on different particle morphologies by Alikarami et al. [56], Guo and Su [13]. Since our tests were performed under stress-controlled conditions, the dilatancy changes monotonically with increase in stress ratio and reaches critical state.

6 Effect of intermediate principal stress ratio

In these set of experiments, the octahedral shear stress at the critical state decreased with increase in 'b' and reached a minimum at $b = 1$ immaterial of the particle morphology. Both the material system showed increased contractivity with increase in intermediate principal stress ratio. A 20% reduction in the critical state friction angle (φ_c) from the compression plane ($b = 0$) to the extension plane ($b = 1$) was observed in both the model systems. This friction angle is highest under plane strain conditions (as also identified by Oda and Iwashita [57], Guo and Su [13], Nouguier-Lehon et al. [33]). Figure 5 shows the variation of φ_c obtained from the experiments performed on both the model material systems at different 'b' and calibrated with Lade isotropic single hardening failure criterion (Eq. 4—[58]).

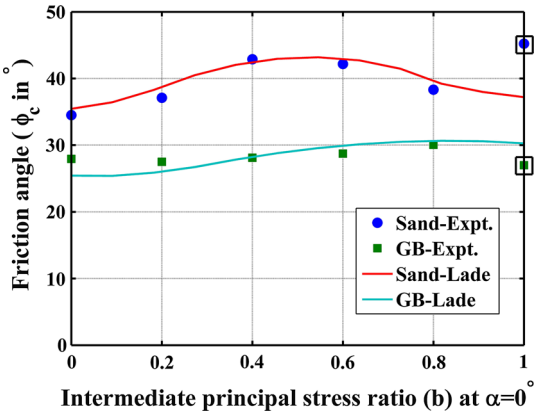

Fig. 5 Angle of internal friction at critical state for both glass ballotini and sand calibrated with Lade isotropic failure criterion. Specimens tested at $b = 1$ did not show a clear critical state

$$\left(\frac{I_1^3}{I_3} - 27\right)\left(\frac{I_1}{P_a}\right)^m = \eta \tag{4}$$

where I_1 and I_3 are the first and third stress invariants of the stress tensor. The Lade's model parameters 'm' and 'η' governs the curvature and the apical angle of the failure surface respectively. The Lade's failure parameters that are used to show the variation of friction angle with 'b' are $\eta = 37.36$ and 14.72 while m = 0.16 and 0.12 for sand and glass ballotini respectively.

A clear increase in critical state friction angle under plane strain conditions was observed in case of angular sand. However, this increase is less pronounced in case of glass ballotini. The critical state friction angle (φ_c) of the angular particles show 20% higher values at $b = 0$ (triaxial condition) compared to glass ballotini and increases to 34% at $b = 0.4$ (plane strain condition). This dependence of critical state friction angle on the individual particle morphology is reflected in a 20% decrease (triaxial case) in φ_c with increase in particle sphericity/form as reported by Guo and Su [13].

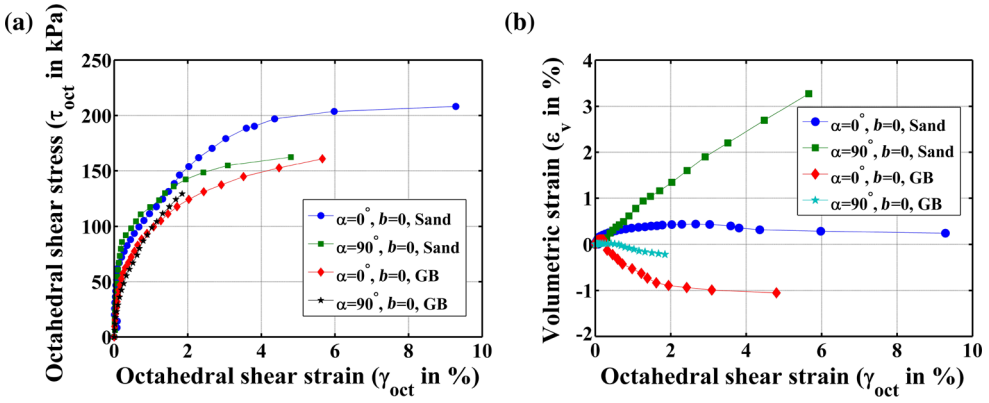

Fig. 6 **a** The decrease in critical state stress and increase in contractivity with increase in principal stress inclination was observed in both the model material systems. The critical state stresses for glass ballotini was lower than sand. **b** Glass ballotini possesses a completely dilative response (negative sign for dilation) compared to that of sand

7 Effect of principal stress inclination

Principal stress inclination (α) is the direction of the major principal stress with respect to the vertical axis of the specimen. The expression for calculating 'α' given in Eq. 5 below which is used to quantify the induced anisotropy of the granular material.

$$\tan 2\alpha = \frac{2\tau_{z\theta}}{\sigma_z - \sigma_\theta} \tag{5}$$

where $\tau_{z\theta}$, σ_z, σ_θ—shear, axial and tangential stress respectively.

Figure 6a shows the variation of octahedral shear stress with octahedral shear strain for tests conducted at $\alpha = 0°$ and 90°, while $b = 0$. The octahedral shear stress gradually increases and reaches constant value at large strains in sand and glass ballotini for both $\alpha = 0°$ and 90°. Even though the specimens were prepared and tested under similar conditions, the percentage decrease in the critical state stress (τ_{oct} between $\alpha = 0°$ to 90°) was slightly lower in case of rounded glass ballotini (18%) than angular sand (22%). Figure 6b shows the volumetric strain response of the two material system for both $\alpha = 0°$ and 90°. Angular sand showed a contractive behaviour for both $\alpha = 0°$ and 90° while rounded glass ballotini showed a dilative behaviour. However in both the material systems the contractivity increases with increase in principal stress inclination. This response was due to the fact that the contact planes between particles were parallel to the bedding planes and consequently the specimen deforms quite easily when the mobilized plane coincides with the bedding plane [25].

8 Discussion

The primary rationale of this experimental study is to understand the mechanical behavior at an ensemble level; given the constituent particulates have drastically different morphologies. We focus specifically on particle morphology effects in stress–dilatancy, anisotropy and non-coaxiality, and finally the failure characteristics. These two model ensembles used in this research—angular sand and spherical glass ballotini were reconstituted to the same relative density.

Effect of particle morphology on the packing properties and basic mechanical response has been extensively researched through both experiments and simulations [10,11,34,59,60]. The effect of particle morphology on the mechanical behaviour of the ensemble concludes that the strength/ stress ratio/ friction angle increases with increase in angularity of the particles. This increase in strength/ stress ratio is attributed to a higher degree of interlocking (or rotational frustration) in angular particles. Additionally, angular particles try to rearrange and configure themselves into a denser configuration during shearing resulting in lesser sliding contacts, in effect exhibiting a more contractive response. While angular particles show a higher coordination number [28,36], spherical particles rarely show any interlocking, and a lower coordination number. However, these spherical particles ride/slide over each other and its neighbors during shearing [4,13], exhibiting a dilative response from the very outset of the test. We also observe from these experiments that with increase in the sphericity of the particles, the strength of the ensemble reduced, while also showing higher dilation.

Stress–dilatancy relationships, which are a hallmark of granular material predictions account mostly for ensemble density and mean stress (or confining pressures), however, particle level attributes such as size, shape etc. are often not considered. Abbireddy and Clayton [11] have discussed the efficacy of Bolton's stress–dilatancy relationship [61] for a range of particle morphologies. They further suggest that Bolton's relationship can be used for limited range of bulky particulates comprising of sub-angular and sub-rounded shapes, however for particulates that are spherical or

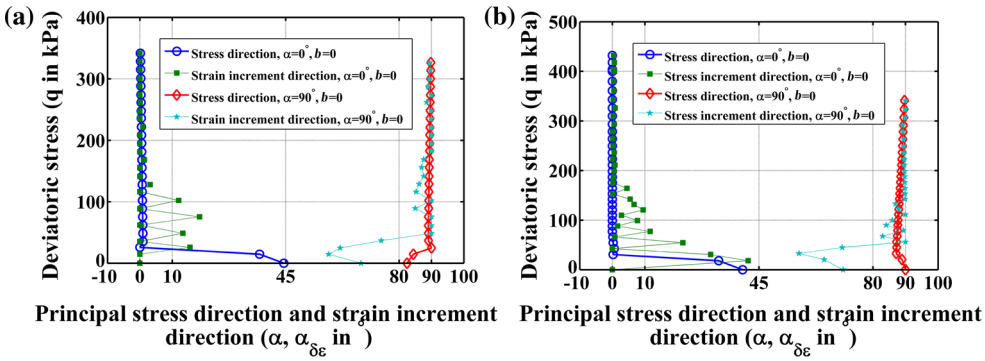

Fig. 7 Variation of principal stress direction and principal strain increment direction for principal stress inclination at 0° and 90°. **a** Glass ballotini. **b** Sand

very platy, Bolton's relationship does not predict the experimentally observed stress–dilatancy response. Guo and Su [13] performed triaxial compression tests on different particle shapes and used the data set to modify the conventional stress–dilatancy relationships to incorporate the effect of inter particle locking for highly angular particles. Cox [4] has also attempted to account for particle morphology in addition to the relative density and confining pressure in stress–dilatancy correlation, empirically through a 'weighted single sand shape parameter (WSSSP)'. This weighted shape parameter was able to reasonably predict the dilatancy. However a rigorous theoretical underpinning in incorporating the effect of particle morphology is still lacking.

Abbireddy and Clayton [11] and Nouguier-Lehon et al. [33] from their experimental results and DEM simulations respectively claim that constant volume shearing or a critical state was not attainable in case of angular particles. However, Pena et al. [59], Azema et al. [36] have shown that granular ensembles indeed reaches a critical state immaterial of the constituent particle morphology. We also observe that a 'critical state' was indeed achieved at large strains, in that, a state of constant shear stress or plastic flow with no corresponding volume change (or near zero dilatancy) was seen in both spherical as well as angular particles.

Anisotropy in a granular ensemble is consequence of the deposition direction vis-à-vis the loading direction. This anisotropy is also affected by the particle morphology, roughness of the particles [26]. Boton et al. [62] suggest that this increase in anisotropy is a consequence of sliding, rolling and dilation of particles relative to the loading direction. Abbireddy and Clayton [11] proposed that when the loading direction is normal to the bedding plane, an increased propensity for particle breakage allows denser packing configuration and in effect also reducing dilatancy. Whilst our results show increase in shear strength and increase in dilatancy when the loading direction is normal to the bedding plane ($\alpha = 0°$) especially for angular particles. It should be noted here that measurement of the grain size before and after the testing did not show much particle breakage during shear. However, the overall anisotropy (measured as RA, as shown in Eq. 6—[26]) reduces from 30% for angular sand to 25% when the particles are spherical in our experiments.

$$RA = \frac{\eta_{max} - \eta_{min}}{\eta_{min}} \tag{6}$$

where η_{max} is the maximum stress ratio which occurs at $\alpha = 0°$ and at critical state in this study, while η_{min}, the minimum stress ratio occurs at $\alpha = 90°$. Experimental studies by Yang et al. [26] also noted that anisotropy exists for both angular and rounded particles; the magnitude is smaller with increase in sphericity. Oda [63] opines that anisotropy not only exists in angular particles but also in spherical particles primarily due to the particle contacts that are different in different directions. DEM simulations of Azema et al. [36] on spherical and polyhedral particles show that the increased strength in angular particle assemblages is primarily due to the increased force anisotropy (due to normal and tangential forces) compared to that of the fabric anisotropy (due to number of contacts and contact length). This increased force anisotropy in angular particles is a result of the increased tortuosity in force distributions and the existence of increased face-face contacts in angular particles.

Non-coaxiality is defined as the non-coincidence of the principal stress direction (α) with the direction of the principal strain increment ($\alpha_{\delta\varepsilon}$) during the plastic deformation. Figure 7a, b shows the variation of principal stress direction and principal strain increment direction (for $\alpha = 0°$ and 90° at $b = 0$) of spherical glass ballotini and angular sand particles respectively. The principal strain increment direction '$\alpha_{\delta\varepsilon}$' at the initial stages of the test was seen to be far more scattered, up until a threshold value of deviatoric stress. This initial scatter in the data is conjectured to be due to the inaccuracies in measurement of strains at low deviatoric stress levels [64]. However with increase in deviatoric stress, the strain increment direction tends to coincide with the stress direction and becomes coaxial well before critical state. We

did not find any significant variation in the response with change in particle shape.

Yang et al. [26] in their extensive investigation on anisotropy and non-coaxiality have concluded from their experiments that the specimens tend to show a coaxial response ($\alpha = 0°$ and $90°$) immaterial of the particle morphology. However, they also suggest that the non-coaxiality exists when tested at other principal stress inclination ($0° < \alpha < 90°$). This non-coaxiality increases with reduction in sphericity of the particles.

9 Strength development

Figure 8 shows the variation of difference in octahedral shear stress between sand and glass ballotini normalized with respect to mean effective normal stress ($\tau_{oct}(sand) - \tau_{oct}(GB))/(p')$ to the octahedral shear strain at $b = 0$ and $b = 1$. All the specimens were sheared at different 'b' under constant mean effective stress (p′) of 300 kPa for both sand and glass ballotini. We observe here that the stresses developed at lower octahedral shear strains for glass ballotini is higher when compared to that of sand. At strains between 0.4 to 0.6% the τ_{oct} of sand begins to increase and continues to increase towards the critical state. The shear stresses developed for 'b' values between 0 and 1 lie in between these two limiting curves. This increased strength of glass ballotini at the initial stages of loading is due the increased number of contacts during shearing (or increase in coordination number due to sliding and rolling over of particles) when compared to that of sand. This also allows the onset of dilatancy under very small strains. On the other hand, in case of angular sands, rearrangement and interlocking of sand particles into a denser configuration occurs under small strain regimes. Azema et al. [36] also show that the number of face-face contacts increases creating a higher degree of interlocking with continued shearing, in effect providing a higher strength and denser configuration to angular particle assemblages than spherical particles. It is also interesting to note that Abbireddy and Clayton [11] further suggest that when particles are platy and angular, dilatancy need not occur in the ensemble, contradicting the classical view of Reynolds that dilatancy is inevitable immaterial of the particle shape.

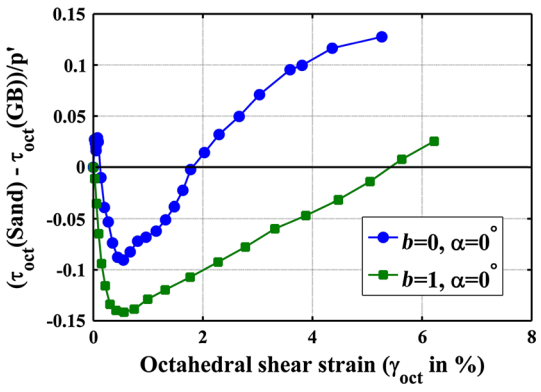

Fig. 8 Variation of octahedral shear stress difference between sand and glass ballotini normalized with respect to mean effective normal stress during the shearing process for $b = 0$ and $b = 1$ at $\alpha = 0°$

10 Failure characteristics

The enhancement of strength due to angularity of the particles at large strains is presented in Figure 9 which is a 2-D representation (a_1/S and a_3/S—Eqs. 7 to 9) of the 3-D stress space where the critical states (the stress state at the end of the test) was plotted for both the particulate systems. This representation of the octahedral plane was obtained by rotating the intermediate principal stress so as to coincide with the hydrostatic axis ($\sigma'_1 = \sigma'_2 = \sigma'_3$), while the other two principal stresses lie on the octahedral plane [1].

$$a_1 = \left(2\sigma'_1\right) - \sigma'_2 - \sigma'_3/\sqrt{6} \tag{7}$$

$$a_3 = \sigma'_3 - \sigma'_2/\sqrt{2} \tag{8}$$

$$S = \sigma'_1 + \sigma'_2 + \sigma'_3 \tag{9}$$

Figure 9 shows the critical state loci obtained for these two particulate ensembles. Only one sector of the octahedral plane was explored, using sixfold symmetry, the entire critical state locus was constructed [19]. The critical state locus was benchmarked with Lade's failure criteria (Eq. 4) [58] to fit the experimental results. Lade's dimensionless constant 'η' were estimated as 37.36 and 14.72 for sand and glass ballotini respectively. In addition to the confining pressure and density, particle morphology also has an influence in controlling the size of the critical state (yield) locus. Accord-

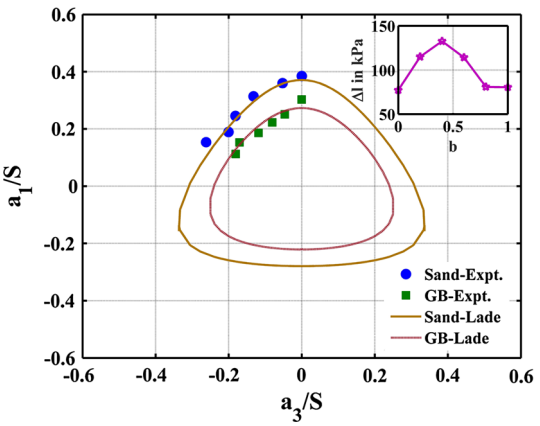

Fig. 9 Change in the size of the critical state locus due to the variation of particle morphology. The experimental points are benchmarked with Lade failure criterion. The inset in this figure shows the distance between the two loci at different intermediate principal stress ratio

ingly, this manifestation of the effect of individual particle morphology, at an ensemble level, can be incorporated by appropriate modification of size of the yield/failure locus.

We further quantify the enhancement in the strength as a 'distance' between the two critical state loci on the octahedral plane (Eq. 10—[65]).

$$\Delta l = \Delta l_{Sand} - \Delta l_{GB} = \left(\sqrt{2J_2}\right)_{Sand} - \left(\sqrt{2J_2}\right)_{GB} \quad (10)$$

where J_2 is the second deviatoric stress invariant. Δl for different 'b', is shown as an inset in Fig. 9. It is observed that Δl = 80 kPa at $b = 0$ and increases with increase in 'b' value up to $b = 0.4$ where Δl = 130 kPa and then decreases. Even though the critical state locus is approximated as smooth concentric loci, small variations exist with changing 'b' value. O'Sullivan et al. [37] suggest an elegant conceptual model to portray the effect of 'b', and suggest that the variation in strength with 'b' is a consequence of buckling of the strong force chains. These DEM simulations indicate the lateral support to the network of strong force chains vary with intermediate and minor principal stress directions, eventually resulting in the reduction of deviatoric stress with increase in 'b'. The authors present the results of two series of simulations performed with two different inter particle friction values, indicating that, the angle of internal friction increases with increase in 'b' upto $b = 0.5$ after which it decreases with 'b'. The particles having a higher inter particle friction exhibited a greater deviatoric strength at critical state. Our results indicate that increase in particle angularity increases the deviatoric strength at a critical state. We draw comparisons between our experiments and the simulations of O'Sullivan et al. [37] in that; particles with higher angularity show similar manifestation at the ensemble level as that of particles with higher inter particle friction (or surface features). Even though these DEM predictions of strength due to increase in inter particle friction and 'b' coincides with the experimental observations, the volumetric responses which are also strongly dependent on inter particle friction or particle morphology has not been discussed.

In summary, the effect of particle morphology on the mechanical behaviour of granular materials has long been recognized as an important feature. In addition to characterization of particle morphology, quantification of mechanical response such as friction angle, non-coaxiality, stress–dilatancy is presented here. Our experiments have been able to quantify this influence of particle morphology through a corresponding change in the size of the yield locus. This is of importance in designing a new or modifying the existing constitutive models. It can also be easily envisioned that results of DEM simulations traditionally carried out on spherical particles can be suitably scaled to particles of various morphologies, if the manifestation at a continuum level is reasonably well established.

11 Summary

This paper presents a series of HCT tests conducted on two model granular ensembles reconstituted to the same relative density, and consolidated to the same effective stress. The critical state locus obtained by conducting tests at different 'b' values indicates that the angular particles exhibit higher strength, i.e. a larger size of the CS locus on an octahedral plane than the spherical particles. Spherical particles exhibit a predominantly dilative behaviour, however present a lower strength at the critical state. The mobilization of strength as a result of rearrangement of angular particles and the consequent interlocking is higher, even with contractive behaviour which is reflected in the higher values of critical state friction angle and the larger size of the yield locus. This effect of individual particle morphology and its manifestation on the critical state behaviour of sand allows incorporating these effects in continuum constitutive models. Another intriguing observation is that during shearing process, the glass ballotini exhibits a greater strength at initial stages. While at larger strains i.e. at critical state, the strength possessed by sand becomes greater than that of the glass ballotini. Finally the overall anisotropy exhibited by angular particles were higher when compared to that of spherical glass ballotini due to increased interlocking and contacts points in case of angular sands. Even though the behavior was coaxial at $\alpha = 0°$ and 90 ° as observed in this study, non-coaxiality exists when tested at other principal stress inclination. Anisotropy and non-coaxiality increases with increase in angularity of the particles.

Appendix

- D_{50}—mean grain size/ median obtained from a particle size distribution (plot between cumulative percentage finer and particle size where the particle size corresponding to 50% finer).
- C_u—uniformity coefficient which is nothing but the ratio between D60 (particle size corresponding to 60% finer obtained from the grain size distribution plot) to D10 (particle size corresponding to 10% finer obtained from the grain size distribution plot). $C_u = \frac{D_{60}}{D_{10}}$
- C_c—coefficient of curvature. $C_u = \frac{D_{30}^2}{D_{60}D_{10}}$ (D30—particle size corresponding to 30% finer obtained from a grain size distribution plot).
- Void ratio (e) is the ratio of volume of voids to the volume of solids.
- Porosity (n) is the ratio of volume of voids to the total volume.
- Packing fraction $\chi = \frac{1}{1+e}$.

Sayao and vaid [50]—Criteria put forth to fix the specimen dimensions so as to minimize non-uniformities.

The specimen geometry is fixed such that the stress distribution across the wall is kept as uniform as possible i.e. the stress difference between real and calculated values should be minimized. In order to fix the dimensions of the hollow cylinder specimen, extensive numerical studies have been carried out using both elastic and plastic formulations to arrive at various sample dimensions.

The criterion proposed by Sayao and Vaid [50] in fixing the specimen geometry is given below:

1. Inner radius: $0.65 \leq \frac{r_i}{r_o} \leq 0.82$
2. Height: $1.8 \leq \frac{H}{2r_o} \leq 2.2$
3. Wall thickness: $r_o - r_i$ = 20 to 60 mm

where r_i—internal radii of the specimen (mm), r_o—external radii of the specimen (mm), H is the height of the specimen (mm). The above criteria can be used when the sand specimen volume is sufficiently large compared to the volume change during shearing, the density is uniform across the wall and the wall thickness should be large compared to the maximum grain size so that the failure mechanism would not be constrained.

Pressure ratio at the end of each test:

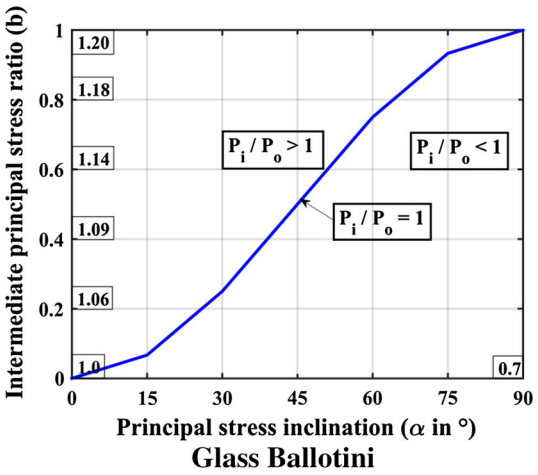

Glass Ballotini

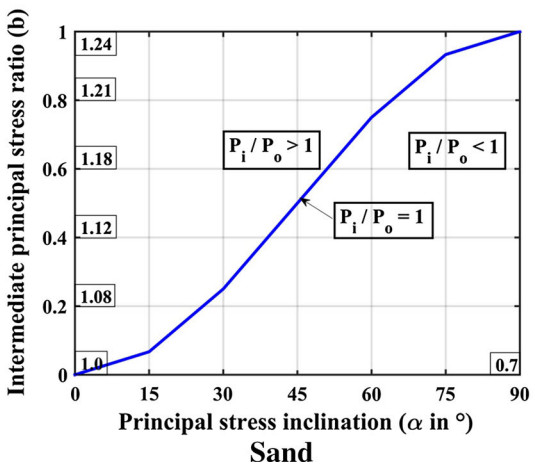

Sand

Equations:

$$\overline{\sigma_z} = \frac{W}{\pi\left(r_o^2 - r_i^2\right)} + \frac{\left(p_o r_o^2 - p_i r_i^2\right)}{\left(r_o^2 - r_i^2\right)} \tag{11}$$

$$\overline{\sigma_r} = \frac{(p_o r_o + p_i r_i)}{(r_o + r_i)} \tag{12}$$

$$\overline{\sigma_\theta} = \frac{(p_o r_o - p_i r_i)}{(r_o - r_i)} \tag{13}$$

$$\overline{\tau_{\theta z}} = \frac{3.M_T}{2.\pi\left(r_o^3 - r_i^3\right)} \tag{14}$$

$$\overline{\varepsilon_z} = \frac{\Delta H}{H} \tag{15}$$

$$\overline{\varepsilon_r} = -\frac{(u_0 - u_i)}{(r_0 - r_i)} \tag{16}$$

$$\overline{\varepsilon_\theta} = -\frac{(u_0 + u_i)}{(r_0 + r_i)} \tag{17}$$

$$\overline{\gamma_{\theta z}} = -\frac{2\beta\left(r_o^3 - r_i^3\right)}{3H\left(r_o^2 - r_i^2\right)} \tag{18}$$

$$\sigma_1 = \frac{\sigma_z + \sigma_\theta}{2} + \sqrt{\left(\left(\frac{\sigma_z - \sigma_\theta}{2}\right)^2 + (\tau_{\theta z})^2\right)} \tag{19}$$

$$\sigma_3 = \frac{\sigma_z + \sigma_\theta}{2} - \sqrt{\left(\left(\frac{\sigma_z - \sigma_\theta}{2}\right)^2 + (\tau_{\theta z})^2\right)} \tag{20}$$

$$p' = \frac{\sigma_1' + \sigma_2' + \sigma_3'}{3} \tag{21}$$

$$q = \frac{1}{\sqrt{2}}\left[\left(\sigma_1' - \sigma_2'\right)^2 + \left(\sigma_2' - \sigma_3'\right)^2 + \left(\sigma_3' - \sigma_1'\right)^2\right]^{1/2} \tag{22}$$

$$\tau_{oct} = \frac{1}{3}\left[\left(\sigma_1' - \sigma_2'\right)^2 + \left(\sigma_2' - \sigma_3'\right)^2 + \left(\sigma_3' - \sigma_1'\right)^2\right]^{1/2} \tag{23}$$

$$J_2 = \frac{1}{6}\left[\left(\sigma_1' - \sigma_2'\right)^2 + \left(\sigma_2' - \sigma_3'\right)^2 + \left(\sigma_3' - \sigma_1'\right)^2\right] \tag{24}$$

$$J_3 = \frac{1}{27}\left[\left(\sigma_1' - \sigma_2'\right)^2\left(\sigma_1' + \sigma_2' - 2.\sigma_3'\right) + \left(\sigma_2' - \sigma_3'\right)^2\left(\sigma_2' + \sigma_3' - 2.\sigma_1'\right) + \left(\sigma_3' - \sigma_1'\right)^2\left(\sigma_3' + \sigma_1' - 2.\sigma_2'\right)\right] \tag{25}$$

$$q = \sqrt{3.J_2}(\text{ for TX-C and TX-E } q = \sigma_1 - \sigma_3) \tag{26}$$

$$\gamma_{oct} = \frac{2}{3}\left[(\varepsilon_1 - \varepsilon_2)^2 + (\varepsilon_2 - \varepsilon_3)^2 + (\varepsilon_3 - \varepsilon_1)^2\right]^{1/2} \tag{27}$$

Relative density,

$$R.D_r = \frac{e_{\max} - e_{nat}}{e_{\max} - e_{\min}} \tag{28}$$

$$\varepsilon_v = \varepsilon_1 + \varepsilon_2 + \varepsilon_3 \tag{29}$$

$$\varepsilon_q = \frac{\sqrt{2}}{3}\left[(\varepsilon_1 - \varepsilon_2)^2 + (\varepsilon_2 - \varepsilon_3)^2 + (\varepsilon_3 - \varepsilon_1)^2\right]^{1/2} \tag{30}$$

u_o is the external radial displacement, u_i is the internal radial displacement, ε_z is the axial strain, ε_r is the radial strain, ε_θ is the circumferential strain, $\gamma_{\theta z}$ is the shear strain, β is the rotation angle, H is the initial height of the specimen, ΔH is the change in axial displacement, p' is the mean effective stress, q is the three dimensional form of deviatoric stress, J_2 is the second deviatoric stress, invariant, J_3 is the third deviatoric stress invariant, τ_{oct} is the octahedral shear stress, γ_{oct} is the octahedral shear strain, e_{max}—maximum void ratio the material can achieve, e_{min}—minimum void ratio the material can achieve, e_{nat}—void ratio at which the specimen is prepared, ε_v—volumetric strain and ε_q—deviatoric strain.

References

1. Rao, K.K., Nott, P.R.: An Introduction to Granular Flow. Cambridge University Press, Cambridge (2008)
2. Terzaghi, K.: Principles of soil mechanics: V-physical differences between sand and clay. Eng. News Rec. **95**(26), 912–915 (1925)
3. Barrett, P.J.: The shape of rock particles, a critical review. Sedimentology **27**(3), 291–303 (1980)
4. Cox, M.R.B.: The influence of grain shape on dilatancy. Ph.D thesis, The University of Arizona (2008)
5. Cavaretta, I: The influence of particle characteristics on the engineering behavior of granular materials. PhD thesis, Imperial college London (2009)
6. Holubec, I., D'Appolonia, E.: Effect of particle slope on the engineering properties of granular soils. In: ASTM Special Technical Publications, vol. 523, pp. 304–318 (1973)
7. Miura, K., Maeda, K., Furukawa, M., Toki, S.: Physical characteristics of sand with different primary properties. Soils Found. **37**(3), 53–64 (1997)
8. Cho, G.C., Dodds, J., Santamarina, J.C.: Particle shape effects on packing density, stiffness, and strength: natural and crushed sands. J. Geotech. Geo Environ. Eng. **132**(5), 591–602 (2006)
9. Santamarina, J.C., Cho, G.C.: Soil behaviour: the role of particle shape. In: Advances in Geotechnical Engineering. The Skempton Conference, vol. 1. Thomas Telford, London, pp. 604–617 (2004)
10. Shin, H., Santamarina, J.C.: Role of particle angularity on the mechanical behavior of granular mixtures. J. Geotech Geo Environ. Eng. **139**(2), 353–355 (2013)
11. Abbireddy, C.O.R., Clayton, C.R.I.: The impact of particle form on the packing and shear behaviour of some granular materials: an experimental study. Granular Matter **17**(4), 427–438 (2015)
12. Tsomokos, A., Georgiannou, V.N.: Effect of grain shape and angularity on the undrained response of fine sands. Can. Geotech. J. **47**, 539–551 (2010)
13. Guo, P., Su, X.: Shear strength, interparticle locking and dilatancy of granular materials. Can. Geotech. J. **44**, 579–591 (2007)
14. Casagrande, A., Carillo, N.: Shear failure of anisotropic materials. Proc. Boston Soc. Civ. Eng. **31**, 74–87 (1944)
15. Arthur, J.R.F., Menzies, K.B.: Inherent anisotropy in a sand. Geotechnique **22**(1), 115–128 (1972)
16. Arthur, J.R.F., Chua, K.S., Dunstan, T.: Induced anisotropy in a sand. Geotechnique **27**(1), 13–30 (1977)
17. Oda, M., Koishikawa, I., Higuchi, T.: Experimental study of anisotropic shear strength of sand by plane strain test. Soils Found. **18**(1), 25–38 (1978)
18. Atkinson, J.H., Bransby, P.L.: The Mechanics of Soils—An Introduction to Critical State Soil Mechanics. Mcgraw Hill Book Co. Ltd, Maidenhead (1982)
19. Davis, R.O., Selvadurai, A.P.S.: Plasticity and Geomechanics. Cambridge University Press, Cambridge (2002)
20. Pietruszczak, S.: Fundamentals of Plasticity in Geomechanics. CRC Press/Balkema, Boca Raton (2010)
21. Dakoulas, P., Sun, Y.: Fine Ottawa sand—experimental behaviour and theoretical predictions. J. Geotech. Eng. (ASCE) **118**(12), 1906–1923 (1992)
22. Kandasami, R.K., Murthy, T.G.: Experimental studies on the influence of intermediate principal stress and inclination on the mechanical behaviour of angular sands. Granular Matter **17**(2), 217–230 (2015)
23. Li, X.S., Dafalias, Y.F.: Anisotropic critical state theory: the role of fabric. J. Eng. Mech. (ASCE) **138**(3), 263–275 (2012)
24. Zhao, J., Guo, N.: Unique critical state characteristics in granular media considering fabric anisotropy. Geotechnique **63**(8), 695–704 (2013)
25. Yang, L.: Experimental study of soil anisotropy using hollow cylinder testing. Ph.D thesis, The University of Nottingham (2013)
26. Yang, Y., Fei, W., Yu, H.S., Ooi, J., Rotter, M.: Experimental study of anisotropy and non-coaxiality of granular solids. Granular Matter **17**(2), 189–196 (2015)
27. O' Sullivan, C.: Particulate Discrete Element Modelling: A Geomechanics Perspective. Taylor & Francis, Hoboken, NJ (2011)
28. Rothenburg, L., Bathurst, R.J.: Micromechanical features of granular assemblies with planar elliptical particles. Geotechnique **42**(1), 79–95 (1992)
29. Peña, A.A., Lizcano, A., Alonso-Marroquin, F., Herrmann, H.J.: Biaxial test simulations using a packing of polygonal particles. Int. J. Numer. Anal. Methods Geomech. **32**(2), 143–160 (2008)
30. Estrada, N., Azema, E., Radjai, F., Taboada, A.: Identification of rolling resistance as a shape parameter in sheared granular media. Phys. Rev. E. **84**(1), 011306 (2011)
31. Azema, E., Radjai, F.: Force chains and contact network topology in sheared packings of elongated particles. Rev. E. **85**(3), 031303 (2012)
32. Saint-Cyr, B., et al.: Particle shape dependence in 2D granular media. Europhys. Lett. **98**(4), 44008 (2012)
33. Nouguier-Lehon, C., Cambou, B., Vincens, E.: Influence of particle shape and angularity on the behaviour of granular materials: a numerical analysis. Int. J. Numer. Anal. Methods Geomech. **27**, 1207–1226 (2003)
34. Azema, E., Radjai, F., Dubois, F.: Packings of irregular polyhedral particles: strength, structure, and effects of angularity. Rev. E **87**(6), 062203 (2013)
35. Azema, E., Estrada, N., Radjai, F.: Nonlinear effects of particle shape angularity in sheared granular media. Rev. E. **86**(4), 041301 (2012)
36. Azema, E., Radjai, F., Saussine, G.: Quasistatic rheology, force transmission, and fabric properties of a packing of irregular polyhedral particles. Mech. Mater. **41**, 729–741 (2009)
37. O' Sullivan, C., Wadee, M.A., Hanley, K.J., Barreto, D.: Use of DEM and elastic stability analysis to explain the influence of the intermediate principal stress on shear strength. Geotechnique **63**(15), 1298–1309 (2013)
38. Abbireddy, C.O.R., Clayton, C.R.I.: Varying initial void ratios for DEM simulations. Géotechnique **60**(6), 497–502 (2010)
39. Kandasami, R.K.: Experimental studies on the mechanical behaviour of cohesive frictional granular materials. Ph.D thesis, Indian Institute of Science (2016)
40. Hight, D.W., Gens, A., Symes, M.J.: The development of a new hollow cylinder apparatus for investigating the effects of principal stress rotation in soils. Geotechnique **33**(4), 355–383 (1983)
41. Krumbein, W.C.: Measurement and geological significance of shape and roundness of sedimentary particles. J. Sediment. Petrol. **11**(2), 64–72 (1941)

42. Powers, M.C.: A new roundness scale for sedimentary particles. J. Sediment. Petrol. **23**(2), 117–119 (1953)
43. Krumbein, W.C., Sloss, L.L.: Stratigraphy and Sedimentation, 2nd edn. Freeman and Company, San Francisco (1963)
44. Okano, J.I., Kikuchi, E., Sasaki, O., Ohi, S.: Geological variation in particle surface roughness preference in the case-bearing caddisflies. Behav. Ecol. Adv. **22**(5), 1053–1063 (2011)
45. ASTM D854: Standard test methods for specific gravity of soil solids by water pycnometer (2010)
46. ASTM D4253: Standard test methods for maximum index density and unit weight of soils using a vibratory table (2006)
47. ASTM D4254: Standard test methods for minimum index density and unit weight of soils and calculation of relative density (2006)
48. Vaid, Y.P., Negussey, D.: Relative density of pluviated sand samples. Soils Found. **24**(2), 101–105 (1984)
49. Cresswell, A., Barton, M.E., Brown, R.: Determining the maximum density of sands by pluviation. Geotech. Test. J. (GTJODJ) **22**(4), 324–328 (1999)
50. Sayao, A., Vaid, Y.P.: A critical assessment of stress non uniformities in hollow cylinder test specimens. Soils Found. **31**(1), 60–72 (1991)
51. Skempton, A.W.: The pore-pressure coefficients A and B. Geotechnique **4**(4), 143–147 (1954)
52. Gutierrez, M., Ishihara, K., Towhata, I.: Flow theory for sand during rotation of principal stress direction. Soils Found. **31**(4), 121–132 (1991)
53. Nakata, Y., Hyodo, M., Murata, H., Yasufuku, N.: Flow deformation of sands subjected to principal stress rotation. Soils Found. **38**(2), 115–128 (1998)
54. Schofield, A., Wroth, C.P.: Critical State Soil Mechanics. McGrow-Hill, London (1968)
55. Been, K., Jefferies, M.: Stress–dilatancy in very loose sand. Can. Geotech. J. **41**, 972–989 (2004)
56. Alikarami, R., Ando, E., Gkiousas-Kapnisis, M., Torabi, A., Viggiani, G.: Strain localisation and grain breakage in sand under shearing at high mean stress: insights from in situ X-ray tomography. Acta Geotech. **10**(1), 15–30 (2015)
57. Oda, M., Iwashita, K.: Mechanics of Granular Materials—An Introduction. Balkema Publishers, Rotterdam (1999)
58. Lade, P.V.: Elasto-plastic stress–strain theory for cohesionless soil with curved yield surfaces. Int. J. Solids Struct. **13**(11), 1019–1035 (1977)
59. Pena, A.A., Garcia-Rojo, R., Herrmann, H.J.: Influence of particle shape on sheared dense granular media. Granular Matter **9**(3–4), 279–291 (2007)
60. Azema, E., Radjai, F., Saint-Cyr, B., Delenne, J.Y., Sornay, P.: Rheology of three-dimensional packings of aggregates: microstructure and effects of non-convexity. Phys. Rev. E **87**(5), 052205 (2013)
61. Bolton, M.D.: The strength and dilatancy of sands. Geotechnique **36**(1), 65–78 (1986)
62. Boton, M., Azema, E., Estrada, N., Radjai, F., Lizcano, A.: Quasistatic rheology and microstructural description of sheared granular materials composed of platy particles. Phys. Rev. E **87**(3), 032206 (2013)
63. Oda, M.: Anisotropic strength of cohesionless sands. J. Geotech. Geoenviron. Eng. (ASCE) **107**, 1219–1231 (1981)
64. Cai, Y., Yu, H., Wanatowski, D., Li, X.: Non-coaxial behavior of sand under various stress paths. J. Geotech. Eng. (ASCE) **139**(8), 1381–1395 (2013)
65. Woo, S.I., Salgado, R.: Determination of an image point on a surface based on a π plane-based algorithm. Comput. Mech. **53**(5), 1033–1046 (2014)